Ultrafine $Co_{1-x}S$ Nanoparticles Embedded in Nitrogen Doped Porous Carbon Hollow Nanosphere Composite as Anode for Superb Sodium-Ion Batteries and Lithium Ion Batteries

Caifu Dong[a], Lijun Guo[a], Yanyan He[a], Limei Shang[a], Yitai Qian[*, a] and Liqiang Xu[*a,b]

[a] Key Laboratory of the Colloid and Interface Chemistry, Ministry of Education, and School of Chemistry and Chemical Engineering, Shandong University, Jinan, 250100, P.R. China

[b]State Key Laboratory of Coordination Chemistry, Nanjing University, P.R. China

Content

Figure captions:

Fig. S1. Typical SEM (a) and TEM (b) images of the obtained material without of 2-methylimidazole addition.

Fig. S2. EDS spectra of $Co_{1-x}S$ (a), $Co_{1-x}S$@C (b) and $Co_{1-x}S$/C (c).

Fig. S3. TGA curves for the $Co_{1-x}S$, $Co_{1-x}S$@C and $Co_{1-x}S$/C between room temperature and 650 ˚C measured with a heating rate of 5 ˚C /min under air atmosphere.

Fig. S4. Typical TEM images of the obtained materials using different amounts (mg) of 2-methylimidazole addition (a) 0, (b) 16.4, (c) 39.4, (d) 65.6, (e) 124.8, (f) 147.8 mg.

Fig. S5. The effect of different reaction time on the morphology of the materials (a) 12 h, (b) 6 h, (c) 30 min. Effect of different reaction temperature on morphology, (d) 50 ºC (e) 70 ºC.

Fig. S6. (a) FT-IR spectra of the materials obtained by adding different amounts (mg) of 2-methylimidazole, (Ⅰ) 2-methylimidazole, (Ⅱ) thiosemicarbazide, (Ⅲ) 0, (Ⅳ) 39.4, (Ⅴ) 124.8. (b) XRD patterns of the as-prepared samples when the amount of 2-methylimidazole was 0 mg (Ⅰ), 39.4 mg, (Ⅱ) and 124.8 mg (Ⅲ) after reaction 72 h.

Fig. S7. EDS spectra of adding different amounts (mg) of 2-methylimidazole, (a) 39.4 (b) 65.6 (c) 124.8.

Fig. S8. The effect of different sulfur sources on the morphology of the material when the amount of 2-methylimidazole was added 124.8 mg (a) thiourea, (b) thioacetamide. The effect of metal salt anions on the morphology of the material when the amount of 2-methylimidazole was 124.8 mg, (c) $CoSO_4 \cdot 7H_2O$, (d) $Co(CH_3COO)_2 \cdot 4H_2O$, (e) $CoCl_2 \cdot 6H_2O$.

Fig. S9. The effect of different sulfur sources on the morphologies of the solid spheres morphology (a) thiourea, (b) thioacetamide.

Tab. S1. The overview diagram of the precursors under different conditions (means using different S resource, Cobalt source, temperature, and time different amounts of 2-methylimidazole (mg)).

Fig. S10. Effect of Ni-doping on material morphology, (a) Co^{2+}: Ni^{2+}=15: 1, (b) Co^{2+}: Ni^{2+}=10: 1, (c) Co^{2+}: Ni^{2+}=5: 1.

Fig. S11. EDS spectra of Ni-doped precursor.

Fig. S12. TEM and SEM images of Ni-doped $Co_{1-x}S$ precursor@PPy.

Fig. S13. (a) Electrolyte optimization of $Co_{1-x}S$-Na batteries. TEM images of $Co_{1-x}S$ (b), $Co_{1-x}S$/C (c) and $Co_{1-x}S$@C (d) obtained after 30 cycles at current density of 500 mA g^{-1}.

Fig. S14. Electrochemical performance of $Co_{1-x}S$, $Co_{1-x}S$/C and $Co_{1-x}S$@C electrodes at 100 mA g^{-1}.

Fig. S15. TEM images of $Co_{1-x}S$@C and $Co_{1-x}S$/C obtained after 120 cycles at current density of 500 mA g^{-1}.

Fig. S16. Cyclic voltammetry (CV) curves of $Co_{1-x}S$ (a) and $Co_{1-x}S$@C (b).

Tab. S2. Electrochemical performance comparisons of the $Co_{1-x}S/C$ electrode with some typical transition metal chalcogenides anode materials for SIBs.

Fig. S17. (a) Charge capacities of Ni-doped $Co_{1-x}S/C$ electrode at 500 mA g^{-1}. (b) Rate capabilities of the Ni-doped $Co_{1-x}S/C$ electrode (charge capacity).

Fig. S18. The electrochemical performance of $Co_{1-x}S/C$ (a) and Ni-doped $_{Co1-x}S/C$ (b) in commonly used carbonate-based electrolyte (1.0 M $NaClO_4$-EC/PC) at the current density of 1000 mAh g^{-1}.

Tab. S3. Electrochemical performance comparisons of the $Co_{1-x}S/C$ electrode with some typical transition metal chalcogenides as anode materials for LIBs.

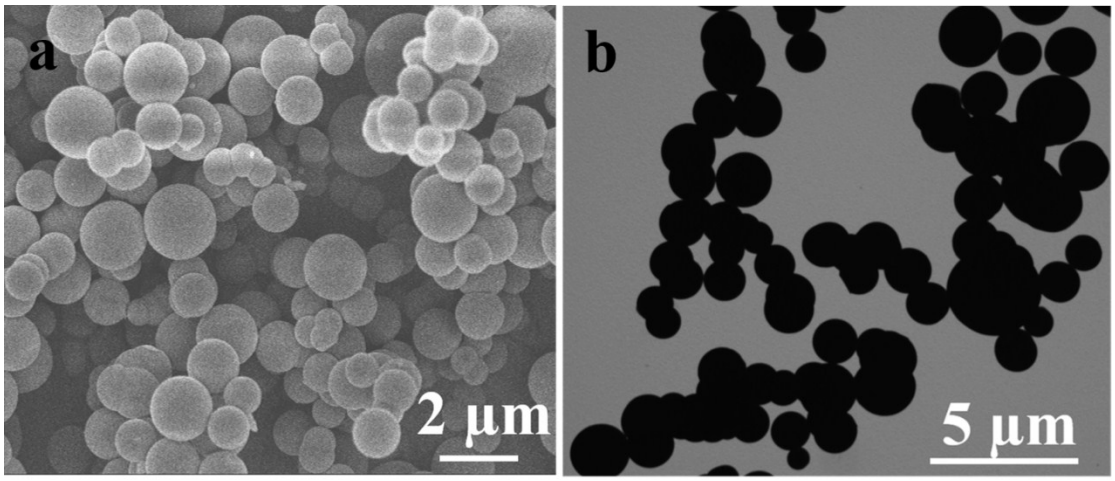

Fig. S1 Typical SEM (a) and TEM (b) images of the obtained material without of 2-methylimidazole addition.

Elements	Atomic presents (%)
Co	8.72
S	16.59
C	58.07
O	15.82
Pt	0.81

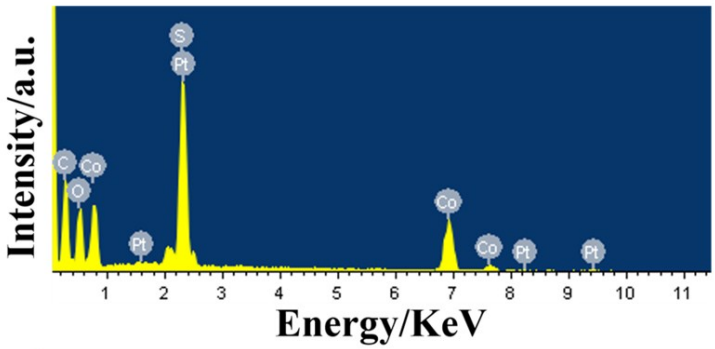

Elements	Atomic presents (%)
Co	6.64
S	10.95
C	75.99
O	5.77
Pt	0.66

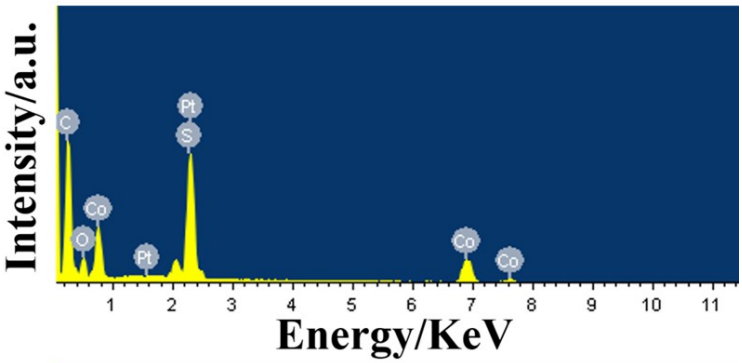

Elements	Atomic presents (%)
Co	4.77
S	7.42
C	77.64
O	9.81
Pt	0.64

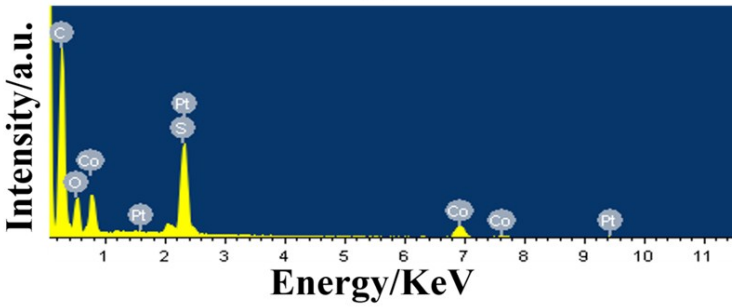

Fig. S2 EDS spectra of $Co_{1-x}S$ (a), $Co_{1-x}S$@C (b) and $Co_{1-x}S$/C (c).

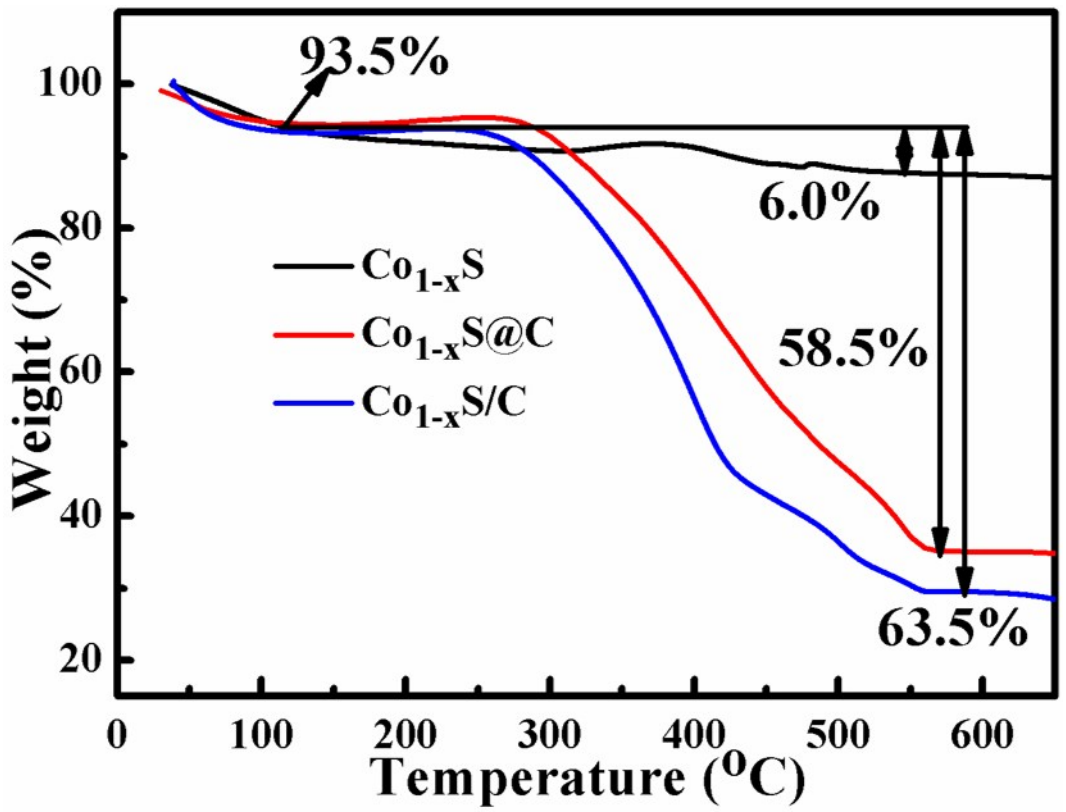

Fig. S3 TGA curves for the $Co_{1-x}S$, $Co_{1-x}S$@C and $Co_{1-x}S$/C between room temperature and 650 ˚C measured with a heating rate of 5 ˚C /min under air atmosphere.

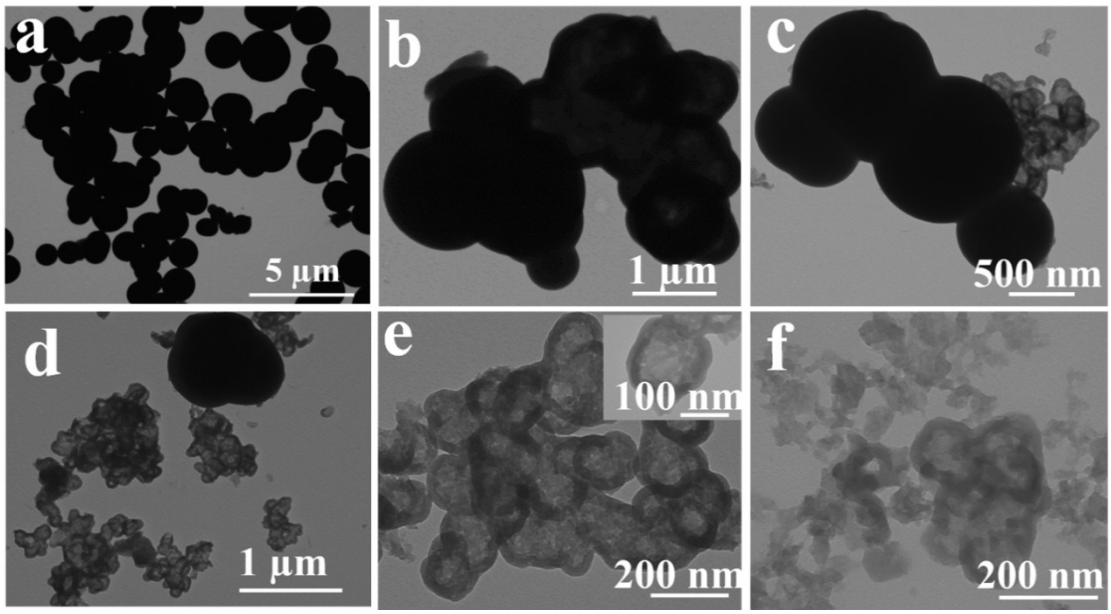

Fig. S4 Typical TEM images of the obtained materials using different amounts (mg) of 2-methylimidazole addition (a) 0, (b) 16.4, (c) 39.4, (d) 65.6, (e) 124.8, (f) 147.8 mg.

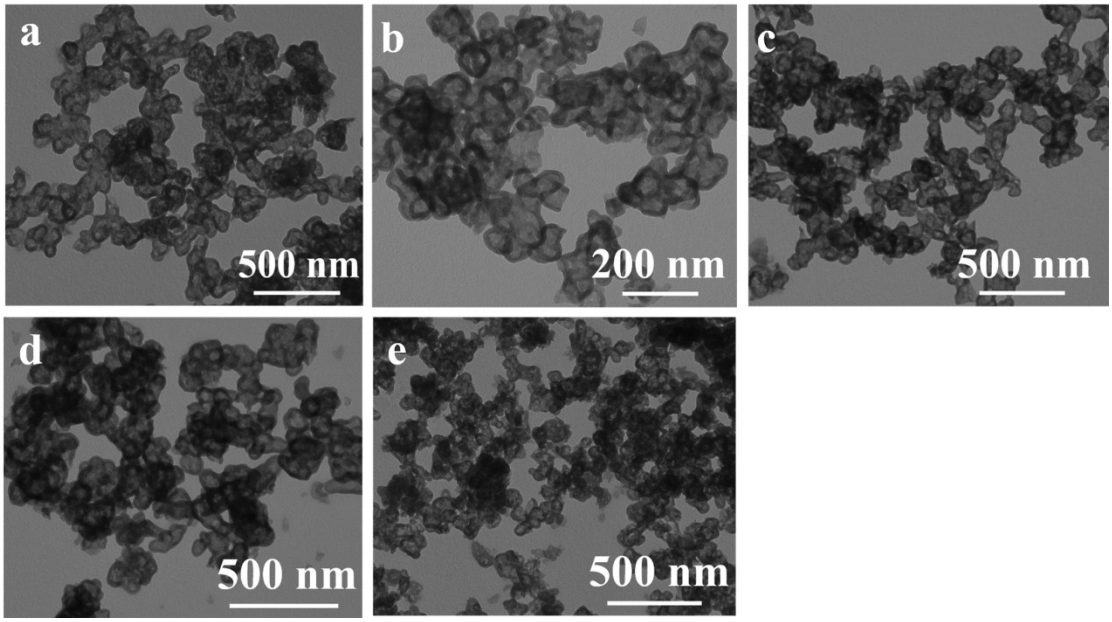

Fig. S5 The effect of different reaction time on the morphology of the materials (a) 12 h, (b) 6 h, (c) 30 min. Effect of different reaction temperature on morphology, (d) 50 ºC (e) 70 ºC.

Time dependent experiments were carried out at 85 ºC. Hollow spheres can obtain after reaction for 12 h, 6 h, even 30 min as shown in Fig. S3 a, b, c. The TEM images (Fig. S3 d, e,) exhibits also can obtain hollow spheres at 70 ºCand 50 ºC after reaction for 30 min. These results show the sphere morphology no obvious dependence on the reaction time and temperature.

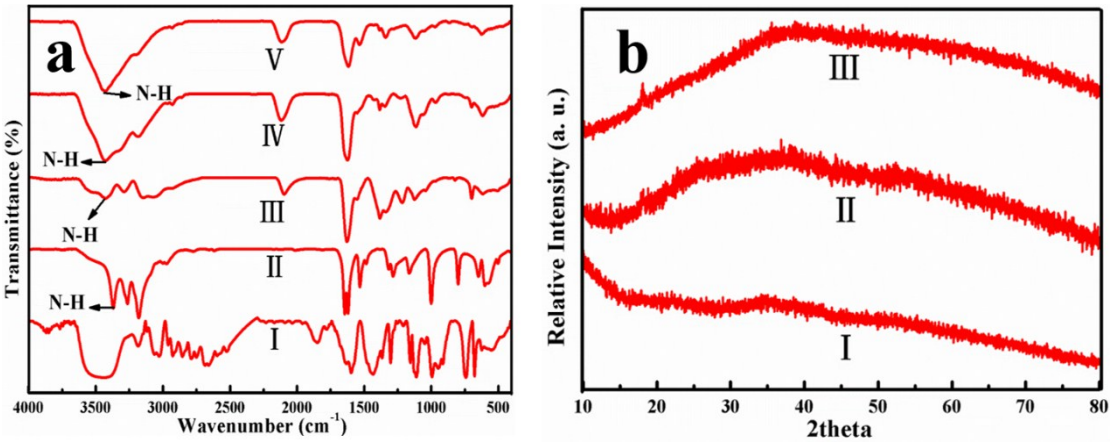

Fig. S6 (a) FT-IR spectra of the materials obtained by adding different amounts (mg) of 2-methylimidazole, (Ⅰ) 2-methylimidazole, (Ⅱ) thiosemicarbazide, (Ⅲ) 0, (Ⅳ) 39.4, (Ⅴ) 124.8. (b) XRD patterns of the as-prepared samples when the amount of 2-methylimidazole was 0 mg (Ⅰ), 39.4 mg, (Ⅱ) and 124.8 mg (Ⅲ) after reaction 72 h.

Elements	Atomic presents (%)
Co	5.19
S	14.93
C	65.41
O	15.67
Pt	1.00

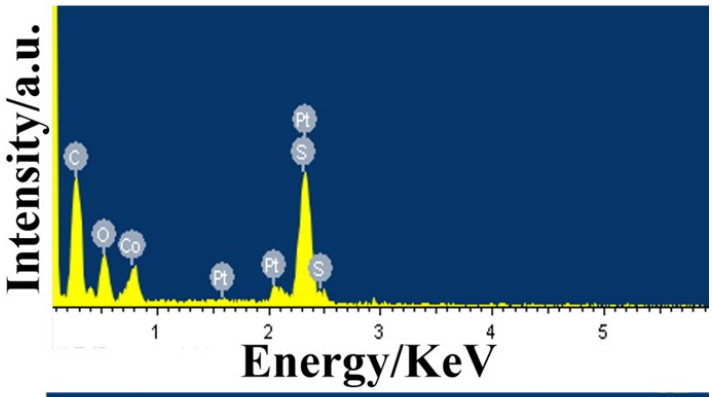

Elements	Atomic presents (%)
Co	6.41
S	12.72
C	63.01
O	14.61
Pt	1.05

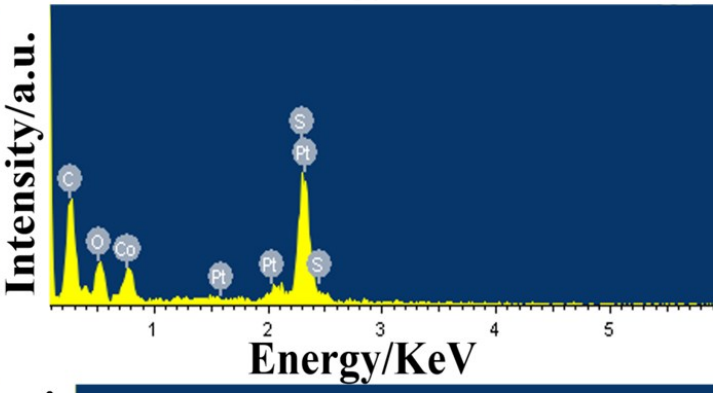

Elements	Atomic presents (%)
Co	4.30
S	10.08
C	69.28
O	15.59
Pt	0.75

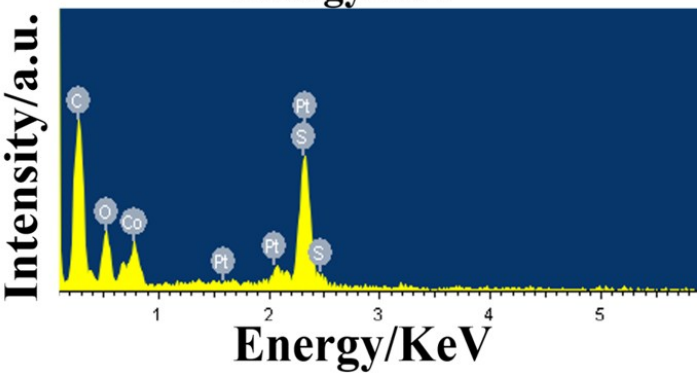

Fig. S7 EDS spectra of adding different amounts (mg) of 2-methylimidazole, (a) 39.4 (b) 65.6 (c) 124.8.

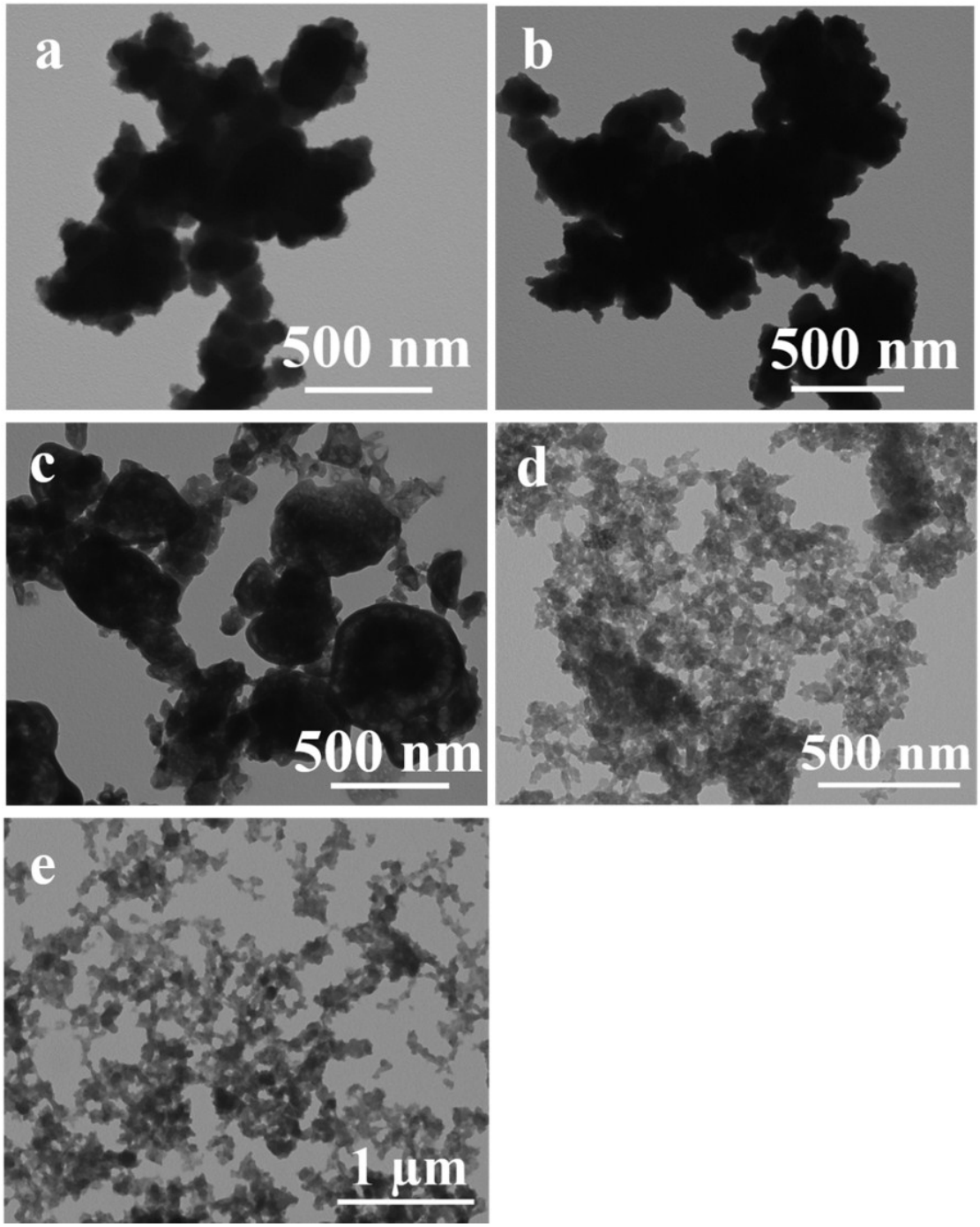

Fig. S8 The effect of different sulfur sources on the morphology of the material when the amount of 2-methylimidazole was added 124.8 mg (a) thiourea, (b) thioacetamide. The effect of metal salt anions on the morphology of the material when the amount of 2-methylimidazole was 124.8 mg, (c) $CoSO_4 \cdot 7H_2O$, (d) $Co(CH_3COO)_2 \cdot 4H_2O$, (e) $CoCl_2 \cdot 6H_2O$.

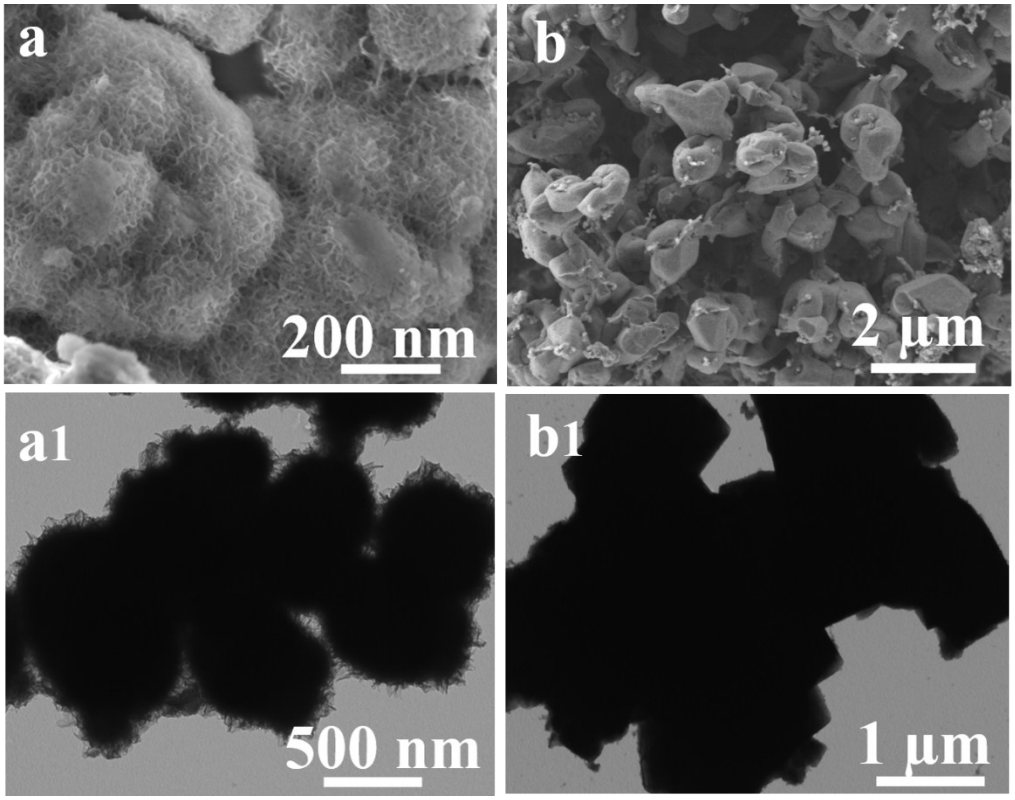

Fig. S9 The effect of different sulfur sources on the morphologies of the solid spheres morphology (a) thiourea, (b) thioacetamide.

Tab. S1 The overview diagram of the precursors under different conditions (means using different S resource, Cobalt source, temperature, and time different amounts of 2-methylimidazole (mg)).

S resource	Cobalt source	2-imidazole (mg)	Temperature (^{O}C)	Time (h)	Morphologies	TEM images
tsc	$Co(NO_3)_2 \cdot 6H_2O$	0	85	72	scattered solid spherical	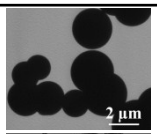
tsc	$Co(NO_3)_2 \cdot 6H_2O$	65.6	85	72	hollow spherical and solid spherical	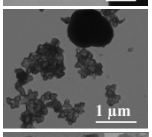
tsc	$Co(NO_3)_2 \cdot 6H_2O$	124.8	85	72	hollow spherical (highest yield)	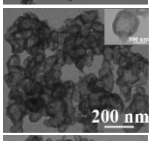
tsc	$Co(NO_3)_2 \cdot 6H_2O$	124.8	85	6	hollow spherical	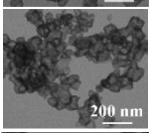
tsc	$Co(NO_3)_2 \cdot 6H_2O$	124.8	85	0.5	hollow spherical	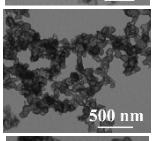
tsc	$Co(NO_3)_2 \cdot 6H_2O$	124.8	70	0.5	hollow spherical	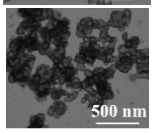
tsc	$Co(NO_3)_2 \cdot 6H_2O$	124.8	50	0.5	hollow spherical	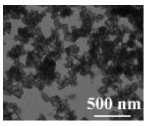
taa	$Co(NO_3)_2 \cdot 6H_2O$	124.8	85	72	Interconnected solid spheres	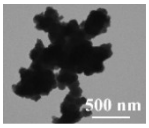
thiourea	$Co(NO_3)_2 \cdot 6H_2O$	124.8	85	72	Interconnected solid spheres	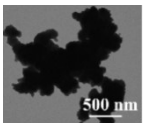
tsc	$CoCl_2 \cdot 6H_2O$	124.8	85	72	Disordered nanosheets	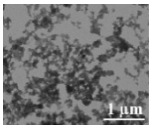
tsc	$CoSO_4 \cdot 7H_2O$	124.8	85	72	Disordered porous nanosheets	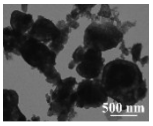
tsc	$Co(CH_3COO)_2 \cdot 4H_2O$	124.8	85	72	Disordered nanosheets	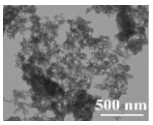

Thioacetamide (taa), thiosemicarbazide (tsc).

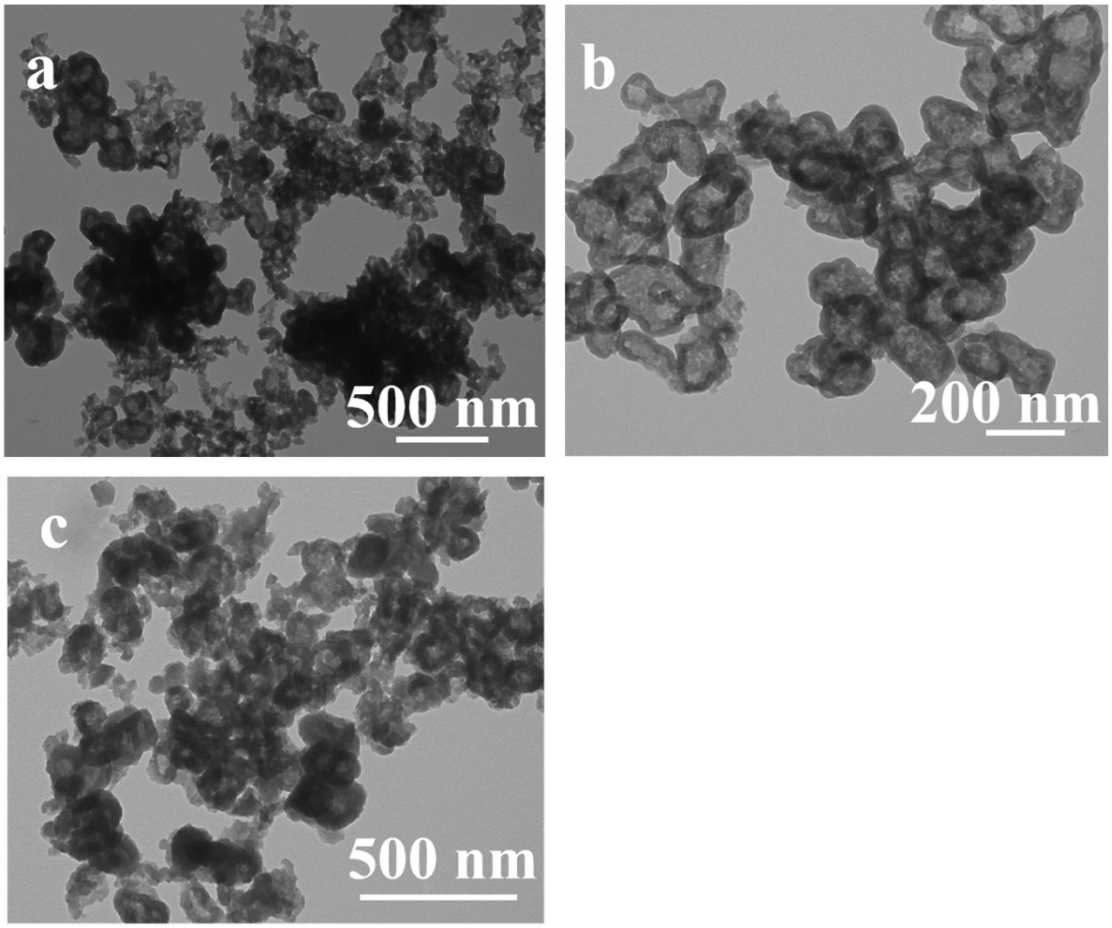

Fig. S10 Effect of Ni-doping on material morphology, (a) Co^{2+}: Ni^{2+}=15: 1, (b) Co^{2+}: Ni^{2+}=10: 1, (c) Co^{2+}: Ni^{2+}=5: 1.

Elements	Atomic presents (%)
Co	6.81
Ni	1.66
S	18.40
C	46.03
O	12.34
Pt	0.77

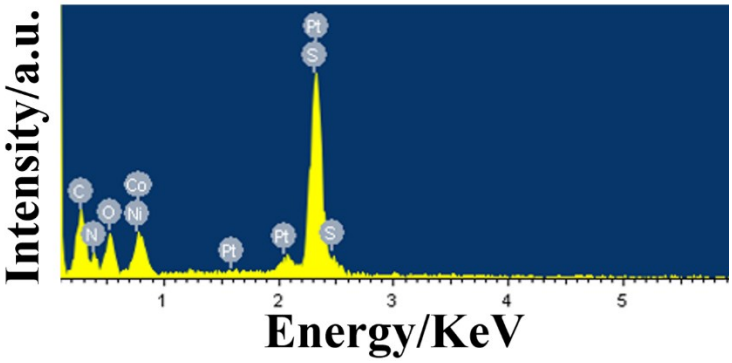

Fig. S11 EDS spectra of Ni-doped precursor.

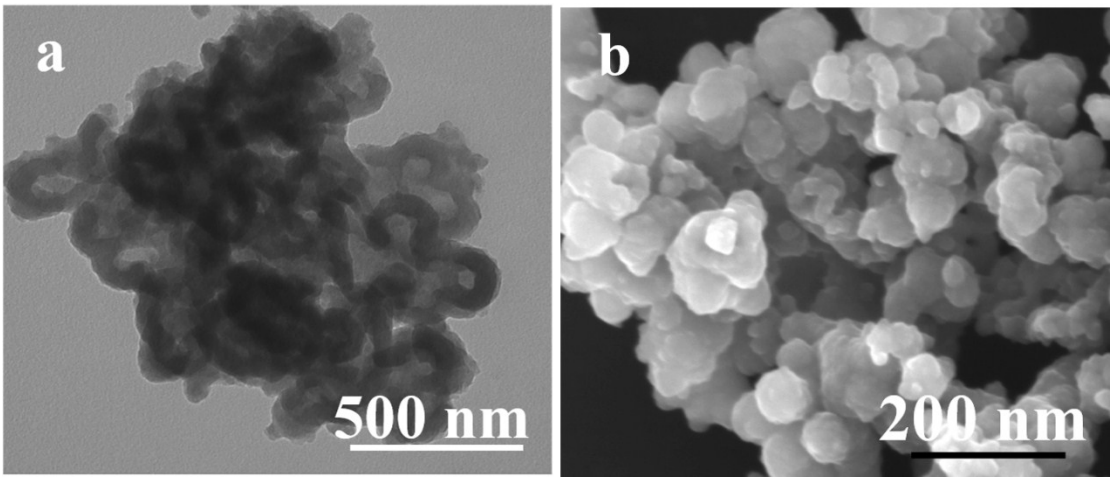

Fig. S12 TEM and SEM images of Ni-doped $Co_{1-x}S$ precursor@PPy.

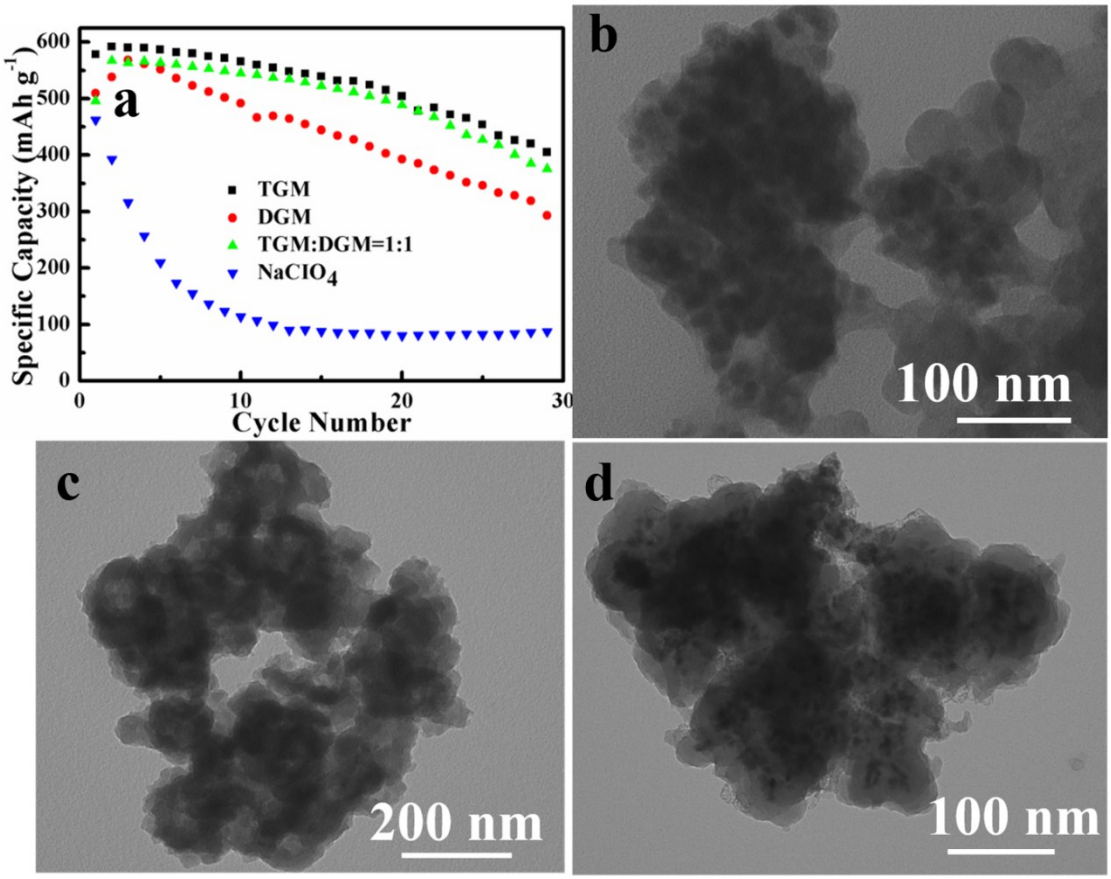

Fig. S13 (a) Electrolyte optimization of $Co_{1-x}S$-Na batteries. TEM images of $Co_{1-x}S$ (b), $Co_{1-x}S/C$ (c) and $Co_{1-x}S@C$ (d) obtained after 30 cycles at current density of 500 mA g^{-1}.

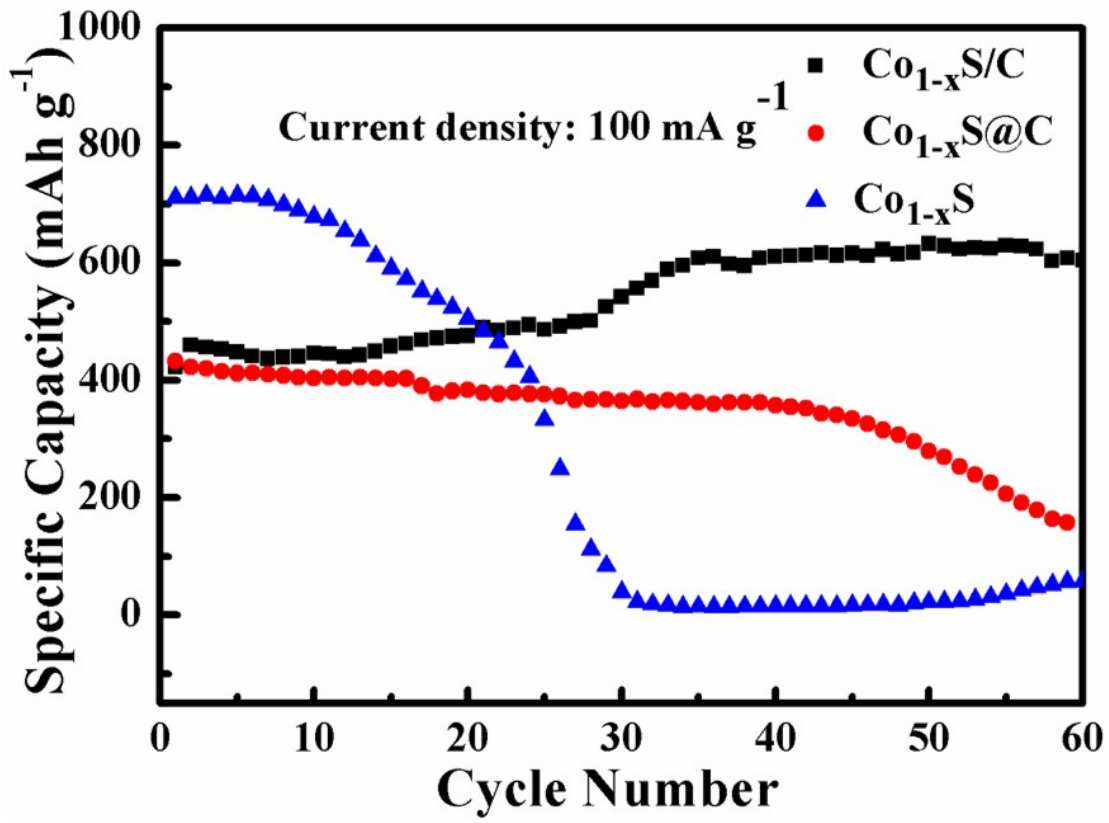

Fig. S14 Electrochemical performance of $Co_{1-x}S$, $Co_{1-x}S/C$ and $Co_{1-x}S@C$ electrodes at 100 mA g^{-1}.

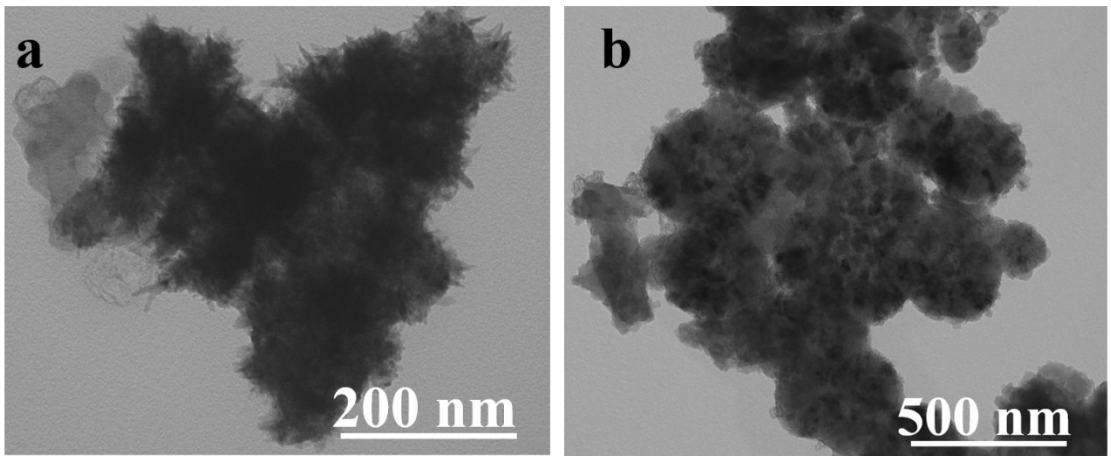

Fig. S15 TEM images of $Co_{1-x}S$@C and $Co_{1-x}S$/C obtained after 120 cycles at current density of 500 mA g^{-1}.

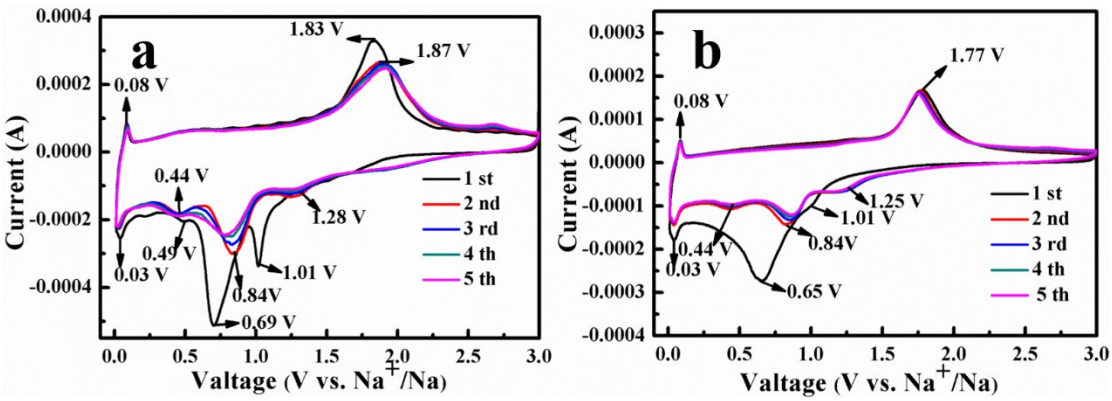

Fig. S16 Cyclic voltammetry (CV) curves of $Co_{1-x}S$ (a) and $Co_{1-x}S$@C (b).

Tab. S2 Electrochemical performance comparisons of the $Co_{1-x}S/C$ electrode with some typical transition metal chalcogenides anode materials for SIBs.

Electrode	Current (mA g^{-1})	Capacity (mA h g^{-1})	Cycle number	Ref/year
Co_3S_4–PNS/GS	500	329	50	1/2015
Co_9S_8–carbon	500	404	50	2/2015
CNT/CoS@C	500	398	200	3/2017
$Co_{1-x}S$/FGNs	1000	251	200	4/2015
Co_3S_4@PANI	200	252.5	100	5/2016
CoS_2/CoS/GC	200	334	100	6/2016
CoS/C nanowires	100	294	100	7/2016
CoS_2/CNTs	100	568	100	8/2015
$Co_{1-x}S/C$	100	601	60	our work
	500/1000	470/326	120/130	

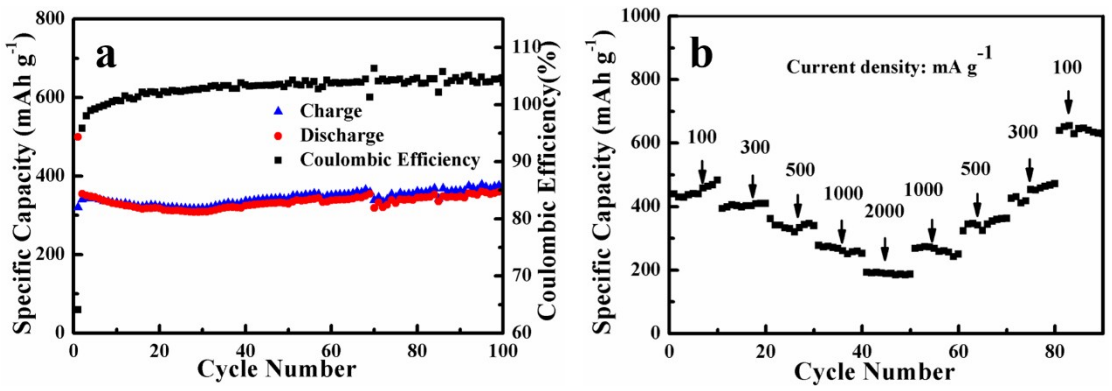

Fig. S17 (a) Charge capacities of Ni-doped $Co_{1-x}S$/C electrode at 500 mA g^{-1}. (b) Rate capabilities of the Ni-doped $Co_{1-x}S$/C electrode (charge capacity).

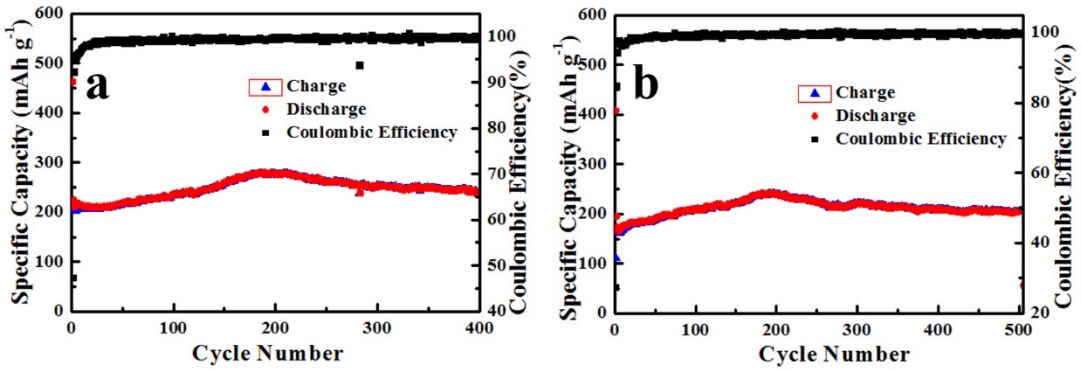

Fig. S18 The electrochemical performance of $Co_{1-x}S/C$ (a) and Ni-doped $Co_{1-x}S/C$ (b) in commonly used carbonate-based electrolyte (1.0 M $NaClO_4$-EC/PC) at the current density of 1000 mAh g^{-1}.

Tab. S3 Electrochemical performance comparisons of the $Co_{1-x}S/C$ electrode with some typical transition metal chalcogenides anode materials for LIBs.

Electrode	Current (mA g^{-1})	Capacity (mA h g^{-1})	Cycle number	Ref/year
C-Co_9S_8	545	370	300	9/2017
$Co_{1-x}S$	100	485	150	10/2014
CoS_2/rGO	50	644	30	11/2014
CoS_2/G	400	400	90	12/2013
CoS_2	50	320	40	13/2011
Ni-Co_9S_8	100	720	100	14/2016
$Co_{1-x}S/C$	100	797	100	our work
	500	559	100	

References

(1) Y. C. Du, X. S. Zhu, X. S. Zhou, L. Y. Hu, Z. H. Dai and J. C. Bao, *J. Mater. Chem. A.* 2015, **3**, 6787−6791.

(2) Y. N. Ko and Y. C. Kang, *Carbon,* 2015, **94**, 85−90.

(3) F. Han, C. Y. J. Tan and Z. Q Gao, *J. Power Sources*. 2017, **339**, 41−50.

(4) T. T. Chen, Y. F. Ma, Q. B. Guo, M. Yang and H. Xia, *J. Mater. Chem. A.* 2017, **5**, 3179−3185.

(5) Q. Zhou, L. Liu, Z. F. Huang, L. G. Yi, X. Y. Wang and G. Z. Cao, *J. Mater. Chem. A.* 2016, **4**, 5505−5516.

(6) J. S. Cho, J. M. Won, J. K. Lee and Y. C. Kang, *Nano Energy,* 2016, **26**, 466−478.

(7) C. Wu, Y. Jiang, P. Kopold, P. A. V. Aken, J. Maier and Y. Yu, *Adv. Mater.* 2016, **28**, 7276−7283.

(8) Z. Shadike, M. H. Cao, F. Ding, L. Sang and Z. W. Fu, *Chem. Commun*. 2015, **51**, 10486−10489.

(9) Y. H. Wang, B. H. Wu, X. Y. He, Y. Y. Zhang, H. Li, Y. Y. Peng, J. Wang and J. B. Zhao, *Electrochimica Acta*. 2017, **230**, 299–307.

(10) S. M. Liu, J. X. Wang, J. W. Wang, F. F. Zhang, F. Liang and L. M. Wang, *CrystEngComm*. 2014, **16**, 814–

819.

(11) Q. M. Su, J. Xie, J. Zhang, Y. J. Zhong, G. H. Du and B. S. Xu, *ACS Appl. Mater. Interfaces*. 2014, **6**, 3016−3022.

(12) J. Xie, S. Y. Liu, G. S. Cao, T. J. Zhu and X, B. Zhao, *Nano Energy*, 2013, **2,** 49–56.

(13) Q. H. Wang, L. F. Jiao, Y. Han, H. M. Du, W. X. Peng, Q. N. Huan, D. W. Song, Y. C. Si, Y. J. Wang and H. T. Yuan, *J. Phys. Chem. C*. 2011, **115**, 8300–8304.

(14) R. C. Jin, J. H. Zhou, G. H. Li and L. X. Yang, *Materials Letters,* 2016, **163**, 183–186.